



Full Text View

[Volume 32, Issue 10 \(October 2002\)](#)

Journal of Physical Oceanography

Article: pp. 2828–2847 | [Abstract](#) | [PDF \(772K\)](#)

Baroclinic Rossby Waves in Irregular Basins^{*}

J. H. LaCasce and Joseph Pedlosky

Woods Hole Oceanographic Institution, Woods Hole, Massachusetts

(Manuscript received September 9, 2001, in final form March 21, 2002)

DOI: 10.1175/1520-0485(2002)032<2828:BRWIIB>2.0.CO;2

ABSTRACT

The properties of baroclinic, quasigeostrophic Rossby basin waves are examined. Full analytical solutions are derived to elucidate the response in irregular basins, specifically in a (horizontally) tilted rectangular basin and in a circular one. When the basin is much larger than the (internal) deformation radius, the basin mode properties depend profoundly on whether one allows the streamfunction to oscillate at the boundary or not, as has been shown previously. With boundary oscillations, modes occur that have low frequencies and, with scale-selective dissipation, decay at a rate less than or equal to that of the imposed dissipation. These modes approximately satisfy the long-wave equation in the interior. Using both unforced and forced solutions, the variation of the response with basin geometry and dissipation is documented. The long-wave modes obtain with scale-selective dissipation, but also with damping that acts equally at all scales. One finds evidence of them as well in the forced response, even when the dissipation is weak and the corresponding free modes are apparently absent.

1. Introduction

Understanding the coupled variability of the ocean and atmosphere is a difficult problem, one which encompasses a wide range of temporal and spatial scales and diverse physical phenomena. Understanding how the atmosphere or ocean varies on its own, under either thermodynamic or mechanical forcing imposed by the other, is a useful first step toward comprehending coupled variability. The following is one in a series of analytical works that seeks to characterize the large-scale, wavelike response in an ocean basin under wind driving.

Wind-driven Rossby waves were first considered by [Stommel and Veronis \(1956\)](#) in the context of an unbounded, stratified ocean. The response in a closed basin was first considered by [Pedlosky \(1965\)](#), who focused on (quasigeostrophic) barotropic waves. Phillips (1966) also calculated the barotropic basin response, as well as that in a two-level model. [Flierl \(1977\)](#) examined quasigeostrophic basin waves in a 1½-layer fluid in a circular basin. The baroclinic problem was revisited by [LaCasce \(2000\)](#) and [Cessi and Primeau \(2001\)](#) in a different parameter range and with a square basin. Recently, Primeau (2001) looked at baroclinic waves in basins, which were not square, with dynamics that were not necessarily quasigeostrophic.

Table of Contents:

- [Introduction](#)
- [The tilted rectangle](#)
- [The circular basin](#)
- [Forced response](#)
- [PV damping](#)
- [Convergence](#)
- [Summary and discussion](#)
- [REFERENCES](#)
- [FIGURES](#)

Options:

- [Create Reference](#)
- [Email this Article](#)
- [Add to MyArchive](#)
- [Search AMS Glossary](#)

Search CrossRef for:

- [Articles Citing This Article](#)

Search Google Scholar for:

- [J. H. LaCasce](#)
- [Joseph Pedlosky](#)

The present work likewise considers wind-forced waves in 1/2 layers (the simplest baroclinic system) in a closed basin. As described below, there are several apparent inconsistencies in the above cited works, and at present it is not clear whether these stem from differences in basin geometry, the choice of parameters, or something else. We will attempt to unify the preceding findings with regards to baroclinic waves. As will be seen, these waves possess several curious properties.

We consider solutions to the linearized quasigeostrophic potential vorticity equation for a layer of fluid above a resting layer (e.g., [Pedlosky 1987](#)):

$$\frac{\partial}{\partial t}(\psi_{xx} + \psi_{yy} - F\psi) + \beta\psi_x = \frac{\nabla \times \tau}{\rho_0 H} - \mathcal{D}, \quad (1)$$

with ψ the velocity streamfunction ($\mathbf{u} = \mathbf{k} \times \nabla\psi$), F the inverse square deformation radius, $\beta = \partial f/\partial y = a$ constant, τ the wind stress, H the depth of the layer, and \mathcal{D} a dissipation.

[Equation \(1\)](#) can be nondimensionalized with the following substitutions (e.g., [Pedlosky 1965](#)):

$$(x, y) = L(x', y'), \quad t = (\beta L)^{-1} t',$$

$$\nabla \times \tau = \frac{\tau_0}{\rho_0 H L} \mathcal{T}, \quad \psi = \frac{\tau_0}{\rho_0 \beta H} \psi',$$

where L is the width of the basin. The resulting equation (dropping primes) is

$$\frac{\partial}{\partial t}(\psi_{xx} + \psi_{yy} - F\psi) + \psi_x = \mathcal{T} - \mathcal{D}, \quad (2)$$

where F has been replaced by FL^2 and \mathcal{D} has also been rescaled. The forcing will be taken to be a propagating, monochromatic wind stress curl; that is, $\mathcal{T} = \cos(kx - \omega t)$. Equivalent dimensional parameter values are given in [LaCasce \(2000\)](#); a frequency of $\omega = 0.001$ corresponds roughly to a period of one year in a Pacific-sized basin.

[Flierl \(1977\)](#) noted (with [McWilliams 1977](#)) that taking $\psi = 0$ on the boundary yields solutions to [\(2\)](#) that do not conserve mass if $F \neq 0$. This defect is remedied by instead taking $\psi = \Gamma(t)$ on the boundary and imposing mass conservation via the integral constraint:

$$\frac{\partial}{\partial t} \iint \psi \, dx \, dy = 0. \quad (3)$$

Allowing $\psi = \Gamma(t)$ at the boundary permits interfacial oscillations, the quasigeostrophic (QG) counterpart of Kelvin waves (the latter possess an infinite phase speed under the QG approximation; see also below). Including boundary oscillations could conceivably alter the solutions greatly, but [Flierl](#) found instead only small changes to the structures and frequencies of the basin normal modes from those with $\psi = 0$ imposed at the boundary.

[Cessi and Primeau \(2001\)](#) and [LaCasce \(2000\)](#) revisited the baroclinic problem, but in a square basin. Both were interested in larger values of F , that is, of basins much larger than the deformation radius (the situation typical in the oceans). Somewhat surprisingly, modes were found that were very different from those with $\psi = 0$ imposed on the boundary. These new modes had large scales and low frequencies; but perhaps most interestingly, they decayed very slowly in the presence of scale-dependent dissipation ([Cessi and Primeau 2001](#)).

The simplest way to see how these slowly decaying modes arise is with solutions to the one-dimensional version of [\(2\)](#) ([LaCasce 2000](#)). The (time periodic) solution with $\psi = 0$ at $x = 0$ and $x = L_x$ is

$$\psi = A \cos\left(\frac{1}{2\omega_n} x - \omega_n t\right) \sin\left(\frac{n\pi x}{L_x}\right), \quad (4)$$

where

$$\omega_n = -\frac{1}{2(n^2\pi^2/L_x^2 + F)^{1/2}}, \quad n = 1, 2, 3, \dots \quad (5)$$

But taking $\Psi = \Gamma(t)$ on the boundary and demanding

$$-i\omega \int_0^{L_x} \psi = 0$$

yields instead

$$\psi = A \cos\left(\frac{2n\pi x}{L_x} - \omega_n t\right) \quad (6)$$

with

$$\omega_n = -\frac{(2n\pi/L_x)}{4n^2\pi^2/L_x^2 + F}, \quad n = 1, 2, 3, \dots \quad (7)$$

$$\text{and } \Gamma = A \cos(\omega_n t). \quad (8)$$

These two solutions are very different. The first, with a westward-propagating wave superimposed on a stationary envelope, is actually the superposition of two free Rossby waves, a long wave with a westward group velocity and a short wave with an eastward group velocity. It is directly comparable to the barotropic normal mode ([Pedlosky 1965](#)), which has the same structure. The contribution from the short Rossby wave makes these modes susceptible to damping because the short-wave group velocity is generally slow. The gravest modes have *high* frequencies [which approach $(2(F))^{1/2}-1$, the maximum free wave frequency] and *short* zonal wavelengths ($L_x \propto F^{-1/2}$).

In contrast, the $\Psi = \Gamma(t)$ solution has only a single free wave component: the long wave with the westward group velocity. It also has an integral number of wavelengths in the basin, thereby matching the oscillatory boundary value (which has equal values at both ends). Here information is returned from the western to the eastern wall via the boundary oscillation, $\Gamma(t)$ and, as such, these modes are less susceptible to damping. In this case the gravest modes have *low* frequencies and *large* zonal wavelengths, exactly the reverse of the $\Psi = 0$ solutions.

The one-dimensional case is simplistic, but qualitatively similar solutions are obtained in the two-dimensional square basin. Why then did [Flierl \(1977\)](#) not observe these modes? Possibly because his values of F were not large enough.

But Flierl also used a *circular* basin. This raises the question of whether the weakly damped modes exist in nonsquare basins. A square basin is special because the time required for the long Rossby wave to cross the interior does not vary with latitude. Indeed, [Primeau \(2001\)](#) suggests that dissipation of the modes that are weakly damped in a square basin increases dramatically when the basin is no longer square. He reasons this is so because the relaying of information via the interfacial oscillation (the “Kelvin wave”) is negatively affected when the wave crests are not parallel to the western boundary. The implication is that weakly damped modes may be less important in irregular basins.

Hereafter we also examine baroclinic waves in irregular basins. By calculating analytical wave solutions in two dimensions, we demonstrate the existence of resonances, even when the the zonal transit times are unequal. The important point is that with large F , the solutions in the basin interior are essentially long Rossby waves, which can by themselves conserve mass; boundary conditions are met in boundary layers. We consider both free modes and the forced response and see, in particular, how understanding the first is helpful but not sufficient for predicting the second. We will also examine different basin geometries, to reassure ourselves of generic characteristics.

2. The tilted rectangle

A good choice for an irregular basin is a trapezoid whose southern boundary width varies ([Primeau 2002](#)); the square basin is recovered when the southern boundary width equals the northern. However, a choice that is more amenable to complete analytical treatment is a rectangular basin that is *tilted*; then the untilted square basin is a special case. As noted, the square has equal zonal transit times but the tilted square obviously does not.¹ The mathematical advantage of the tilted square is that the vorticity equation is still separable. The barotropic normal modes for a tilted rectangular basin were first obtained by [Longuet-Higgins \(1964\)](#).

To solve the problem, we first make a coordinate transformation so that β (rather than the basin) is tilted in the new frame:

$$= \mathcal{T} - \mathcal{D}, \quad (9)$$

where α is the tilt angle. Note the Laplacian is invariant to coordinate rotation, but the traveling wave forcing will now have the form: $\mathcal{T} = \exp\{ik[x \cos(\alpha) - y \sin(\alpha)] - i\omega t\}$.

The free modes occur with zero forcing, $\mathcal{T} = 0$ (forcing is discussed in [section 4](#)). We will also examine two types of dissipation: one proportional to relative vorticity &lsqb=ivalent to purely thermal damping and used by [Cessi and Primeau \(2001\)](#)] and one proportional to potential vorticity [used by [LaCasce \(2000\)](#)]. Relative vorticity (RV) damping selectively removes scales smaller than the deformation radius, while potential vorticity (PV) damping affects all scales equally. With RV damping, $\mathcal{D} = -\delta \nabla^2 \psi$, whereas for PV damping, $\mathcal{D} = -\delta(\nabla^2 \psi - F \psi)$.

With either type of dissipation, [Eq. \(9\)](#) can be reduced to the corresponding inviscid equation. With PV damping, one replaces

$$\tilde{\omega} \leftarrow \omega + i\delta \quad (10)$$

and, with relative vorticity damping, one also replaces

$$\tilde{F} \leftarrow \frac{F\omega}{\omega + i\delta}. \quad (11)$$

Hereafter we will focus on RV damping; PV damping is discussed separately in [section \(5\)](#).

To solve the inviscid equation, we make two substitutions. First,

$$\psi(x, y, t) = \Psi(x, y, t) + \Gamma(t) \quad (12)$$

so that Ψ is zero on the boundaries. Then,

$$\Psi = \Phi e^{-i\kappa[x \cos(\alpha) - y \sin(\alpha)]}, \quad (13)$$

where $\kappa \equiv (2\tilde{\omega})^{-1}$, which changes [Eq. \(9\)](#) to a forced Helmholtz equation:²

$$\phi_{xx} + \phi_{yy} + (\kappa^2 - \tilde{F})\phi = \tilde{F}\Gamma e^{i\kappa[x \cos(\alpha) - y \sin(\alpha)]}, \quad (14)$$

Last, we convert [Eq. \(14\)](#) to an ODE by expanding in a sine series in y ; that is, $\Phi = \sum_{n=1}^{\infty} \phi_n \sin(n\pi y)$ (we assume hereafter the rectangular basin has $L_y = 1$ and $L_x = l$):

$$\frac{\partial^2}{\partial x^2} \phi_n + a_n^2 \phi_n = 2g_n \tilde{F} T e^{i\kappa \cos(\alpha)x}, \quad (15)$$

where $a_n^2 \equiv \kappa^2 - \tilde{F} - n^2\pi^2$ and

$$g_n \equiv \frac{n\pi}{n^2\pi^2 - \kappa^2 \sin^2(\alpha)} [1 - (-1)^n e^{-i\kappa \sin(\alpha)}]. \quad (16)$$

Imposing the boundary conditions on the sum of the particular and homogeneous solutions and then invoking the conservation of mass condition [\(3\)](#) yields a dispersion relation for the basin modes:

$$l + \sum_{n=1}^{\infty} \left\langle \frac{4Fg_n g'_n a_n}{[a_n^2 - \kappa^2 \cos^2(\alpha)]^2} \times \left\{ \frac{\cos(a_n l) - \cos[\kappa \cos(\alpha)l]}{\sin(a_n l)} \right\} + \frac{2Fg_n g'_n l}{a_n^2 - \kappa^2 \cos^2(\alpha)} \right\rangle = 0. \quad (17)$$

Here g'_n is like g_n except that the argument of the exponential in (16) is $+ik \sin(\alpha)$. Resonant frequencies are those that satisfy (17); with dissipation, they are generally complex.

To begin, we consider the untilted square basin; that is, $\alpha = 0$ and $l = 1$, the basin of LaCasce (2000) and Cessi and Primeau (2001). Equation (17) was evaluated for a range of discrete values of $\omega = \omega_r + i\omega_i$; then zeros of (17) were found.

The zeros are shown in Fig. 1, with RV damping, $F = 50$ and $\delta = 0.002$. The modulus of (17) is contoured, with the bulls-eyes indicating where both the real and imaginary parts are simultaneously small. The modes obtained with $\psi = 0$ on the boundary are shown in the upper panel and those with $\psi = \Gamma$ on the boundary in the lower panel.

In both cases, solutions fall on a branch with negative ω_i . The frequencies can be derived for the case with $\psi = 0$ on the boundary. From (15), we have

$$\frac{\partial^2}{\partial x^2} \phi_n + a_n^2 \phi_n = 0$$

so that solutions have $\phi_n \propto \sin(a_n x)$ with

$$a_n l = m\pi.$$

Solving for ω and taking $l = 1$, we obtain

$$\omega = \frac{[(m^2 + n^2)\pi^2 + F - \delta^2 F^2]^{1/2}}{2[(m^2 + n^2)\pi^2 + F]} - i\delta \frac{(m^2 + n^2)\pi^2 + F/2}{(m^2 + n^2)\pi^2 + F}. \quad (18)$$

The real part of ω is thus bounded above by the maximum free wave frequency, $(2(F)^{1/2})^{-1}$. Similarly the imaginary part is negative and bounded below by $-\delta$ and above by $-\delta/2$. The gravest mode has the *largest* real frequency (shortest period) and is also the least damped.

The solutions in the upper panel are in accord with (18). The gravest mode has $\omega = (0.0599, -0.0013)$. The other modes lie in an increasingly dense cluster, with $\omega_i \rightarrow -\delta$ as the mode number increases.

The mode frequencies obtained with $\psi = \Gamma$ on the boundary (lower panel) also fall on a branch, with the imaginary parts again bounded above by $-\delta/2$ and below by $-\delta$. The gravest mode here has $\omega = (0.0602, -0.0012)$, and the streamfunction (not shown) is very similar to that of the gravest mode with $\psi = 0$ on the boundary.

One aspect of the $\psi = \Gamma$ solution is that modes that are asymmetric in y [or have n even in (17)] do not appear as solutions of (17) because they satisfy (3) trivially (Flierl 1977; LaCasce 2000). For this reason, the even n modes were excluded from the top panel of Fig. 1.

Nevertheless the modes appear less densely spaced in the lower panel than in the upper. This is due to a difference in meridional structure. The modes with $\psi = 0$ on the boundary have a sinusoidal y dependence, but the modes with $\psi = \Gamma$ on the boundary are nearly uniform in y because the streamfunction on the eastern wall is constant. The sine transform of a constant has component amplitudes proportional to $(n\pi)^{-1}$ for odd values of n (with the even n modes vanishing, as noted) and, as such, the $n = 1$ contribution dominates; the higher modes act to “fill in” the gaps left by the first mode near the boundaries.

In fact, the modal frequencies are nearly the same as those for the $\psi = 0$ modes with a sine mode 1 structure in y . The small differences in frequency (noted by Flierl 1977) presumably stem from the difference in meridional structure. This also causes the apparent sparseness in the lower panel.

In any case, the situation with $F = 50$ is close to that described by Flierl (1977): the oscillatory boundary condition produces only modest changes in the modes. With $\psi = \Gamma(t)$ on the boundary, the modes do have nearly uniform structure in y , a point not explicitly noted before but which is unsurprising given the uniform displacement of the interface along the boundary.

As noted by Cessi and Primeau (2001), differences between the $\psi = 0$ and $\psi = \Gamma$ resonant frequencies emerge at larger F . Shown in Fig. 2 are the modal frequencies obtained with $F = 2000$. The modes found with $\psi = 0$ again fall on a branch

running between $\omega_i = -\delta/2$ and $-\delta$, although they are more densely packed, consistent with (18). Again, only the modes asymmetric in y are shown.

There are likewise modes with $\Psi = \Gamma$ on the boundary with imaginary frequencies bounded by $-\delta/2$ and $-\delta$; but in addition there are six modes with smaller imaginary frequencies. The gravest mode is that at the upper left in the figure. It has a decay rate that is nearly an order of magnitude less than the imposed damping time and a real frequency that is substantially less than the free wave cutoff. The change in boundary condition has thus decreased both the damping rate and the frequency of the gravest mode, as for the one-dimensional solution discussed in section 1.

The gravest mode structure changes too (Fig. 3). The solution with $\Psi = 0$ on the boundary (upper panel) is notable for its short zonal scales (the westward intensification stems from the negative imaginary part of the frequency). The $\Psi = \Gamma$ solution, on the other hand, has a large zonal wavelength and is nearly one-dimensional with meridional variations occurring mostly in boundary layers at the northern and southern walls.

The change in boundary conditions thus greatly affects the solutions when F is large. So far, our results are in accord with Flierl (1977) at small F and with LaCasce (2000) and Cessi and Primeau (2001) at large F . But the question remains: is there a difference with irregular basins?

Shown in Fig. 4 are solutions to (17) with $F = 2000$ with nonzero values of α . The solution is found as before with zero tilt; however, the sine modes with even n now contribute as well. Shown in the upper panel are modes with a relatively weak tilt ($\alpha = \pi/12$) and in the lower panel those with a larger tilt ($\alpha = \pi/5$). The crosses in both panels represent frequencies obtained with a long-wave solution, explained below. We see immediately the weakly damped modes are present in both cases, indicating they do not require equal zonal transit times.

But the basin shape, however, does affect the modes because the damping rate increases with increasing tilt. One also finds the basin width alters the number of weakly damped modes obtained; with $l = 2$, there are seven rather than five such modes.

How do we rationalize these various findings? The gravest mode frequencies from the long-wave solution (the crosses) are very near those from the full solutions; both solutions also have damping rates which increase with increasing tilt. This suggests that it might be fruitful to first understand the long-wave solution.

a. Long-wave solution

With large values of F and weak (RV) dissipation, one can ignore damping and the variation of relative vorticity in the interior. Then the interior is governed approximately by the long-wave equation:

$$i\omega F\Psi + \cos(\alpha)\Psi_x - \sin(\alpha)\Psi_y = 0. \quad (19)$$

The solution to (19) can be obtained by the method of characteristics. With $\alpha = 0$, the characteristics all emanate from the eastern boundary, but with $\alpha > 0$, some come from the southern boundary, yielding two regions, denoted hereafter “A” and “B,” separated by the line $y = (l - x) \tan(\alpha)$. In the lower region (A), we have

$$\Psi_A = \Gamma \exp[i\omega Fy/\sin(\alpha)] \quad (20)$$

and in the upper region (B),

$$\Psi_B = \Gamma \exp[i\omega F(l - x)/\cos(\alpha)]. \quad (21)$$

Note the two solutions are equal on the separatrix, $y = (l - x) \tan(\alpha)$.

To satisfy the boundary conditions at the western and northern walls requires boundary layers. Including these is straightforward, yielding the corrected solutions:

Again, ω is generally (but not always) complex. Notice that having a western boundary layer requires $\omega_i > -\delta$, a condition always met by the free modes.

With low frequencies and weak damping, the boundary layers occupy only a tiny fraction of the domain and contribute little to the mass integral. It follows that the resonant frequencies are approximately those for which the integral of the long-wave solutions alone vanishes.⁴ Assuming $\alpha < 45^\circ$, we have

$$\int_0^l dx \int_0^{(l-x)\tan(\alpha)} dy \psi_A + \int_0^l dx \int_{(l-x)\tan(\alpha)}^l dy \psi_B = 0, \quad (24)$$

which yields a dispersion relation for the frequency

$$\tan\left[\frac{\omega Fl}{2 \cos(\alpha)}\right] = \frac{\omega Fl \tan(\alpha)}{i\omega F + 2 \sin(\alpha)}. \quad (25)$$

Solutions to relation (25) were obtained numerically and are indicated by the crosses in Fig. 4, as noted. There is also a solution with $\omega_r = 0$, but this has a spatially constant streamfunction, which due to mass conservation is trivially zero. The gravest nontrivial modes have ω_r near 0.003, as do the gravest modes from the full solution.

How does the structure of the full solution compare with that of the long-wave solution? The gravest mode streamfunctions from the full and long-wave solutions for two values of the tilt angle are shown in Fig. 5 and are qualitatively very similar, both in the interior and even near the boundaries (although the sharp corners in the long-wave solutions are smoothed out in the full solutions). Note in both cases there are wiggles in the boundary layers; these stem from a harmonic component in the boundary layer correction and will be found later to affect numerical convergence properties (sec. 6).

Although the long-wave gravest mode frequencies agree well with those from the full solutions, the agreement is less satisfactory for the higher modes, diverging as the real part of the frequency approaches the maximum free wave frequency, $(2F)^{1/2}$. Such a divergence is to be expected for a long-wave solution and, of course, will vary with F . Nevertheless, the structure of the second and third modes (not shown) is quite similar for the two solutions.

b. The untilted square

Given these initial similarities, we can exploit the long-wave solution to understand further aspects of the full solution. First we return to the untilted square basin. When $\alpha = 0$, there is no region A and all characteristics emanate from the eastern boundary. Then

$$\psi_B = \Gamma \exp[i\omega F(l-x)], \quad (26)$$

and the dispersion relation (25) implies

$$\omega = 2n\pi/F \quad (27)$$

[also noted by Primeau (2002)]. Relation (27) implies that there are an integral number of zonal wavelengths in the basin and hence *no boundary layer* at the western wall. In fact, the long-wave solution in the square is one-dimensional: (27) is just the long-wave approximation of (7). This lack of boundary layers obviously influences the dissipation, as discussed next.

c. Dissipation

The long-wave solutions exhibit a subtle dependence on dissipation. The value of ω_i is determined by the basin geometry, not by the (RV) damping coefficient. This geometrical dependence occurs because ω_i alters the spatial distribution of the wave, which in turn affects the vanishing of the mass integral.

For the untilted square basin, $\omega_i = 0$ because mass is conserved simply by having an integral number of waves in the basin. The long-wave solution in the untilted basin is thus *undamped* (or possesses an infinite Q factor; Primeau 2002). But with nonzero tilt, ω_i is negative and, as such, the untilted basin is a singular limit for the long-wave solution.

The modes obtained from the full solution are not similarly inviscid however (recall that $\omega_i < 0$ for all modes; [Fig. 2](#)). This is so because a 2D basin requires boundary layers at the northern and southern walls, even if untilted. The long-wave modes in the full solution are the least damped when the basin is untilted, but the untilted basin is not singularly inviscid.

Consistent with the notion that the long-wave mode decay rate depends on basin geometry but not significantly on the imposed damping rate, the long-wave mode frequencies (from the full solution) do not vary appreciably with δ . On the other hand, there are the “lower branch” modes that *do* depend on δ , with $-\delta < \omega_i < -\delta/2$ ([Fig. 2](#)). It would seem that the upper branch might not be distinguishable from the lower branch if the damping is too weak.

This is the case. Shown in [Fig. 6](#) are (full) solutions for a tilted basin with $\alpha = \pi/10$, $F = 1000$, and various δ . In the upper panel, the dissipation is too weak and only the lower branch of modes is evident (the modal frequencies obtained with the $\Psi = 0$ are similar). But as the dissipation is increased (middle and lower panels), the weakly damped modes emerge above the lower branch.

The imaginary values of the frequency for the long-wave solutions are generally of order F^{-1} , so we require $\delta > F^{-1}$ to observe the resonances [the same condition was postulated by [Cessi and Primeau \(2001\)](#)]. It is not enough to have F large; we must also have sufficient dissipation. We will see the situation is somewhat different with PV damping (sec. 5).

To summarize, the weakly damped modes seen previously in the square basin persist in the tilted rectangular basin and so do not require equal cross-basin transit times. These modes are essentially long waves “driven” by boundary oscillations at the eastern and southern (if $\alpha > 0$) walls with boundary layers at the western and northern (if $\alpha > 0$) boundaries.

One might wonder still whether the rectangular basin [or even the trapezoidal basin of [Primeau \(2002\)](#)] is somehow special. Perhaps Flierl's circular basin is different. To see, we turn to the circular basin.

3. The circular basin

The circular basin presents an interesting case for comparison. For one, it has unequal transit times at different latitudes, like the tilted basin. But second, like the untilted square basin, the circular basin is *meridionally symmetric*, so modes with asymmetric structure about the zonal midline have no displacement at the coasts.

The dispersion relation for circular basin modes is Eq. (15) of [Flierl \(1977\)](#). The dispersion relation with relative vorticity damping is the same, following substitutions [\(10\)](#) and [\(11\)](#):

$$\sum_{n=0}^{\infty} \frac{J_n^2(\alpha) J_n'[(\alpha^2 - \tilde{F})^{1/2}]}{(1 + \delta_{n0}) J_n[(\alpha^2 - \tilde{F})^{1/2}]} = 0, \quad (28)$$

where J_n is the Bessel function of integral order; the prime indicates a derivative with respect to the argument, $\delta_{n0} = 1$ only if $n = 0$ and where $\alpha = [2(\omega + i\delta)]^{-1}$.

We found solutions to [\(28\)](#) numerically. The only difference from Flierl's original calculation is that we consider larger F and include RV damping. A representative case (with $F = 1000$) is shown in [Fig. 7](#).

Exactly as in the rectangular basin, there are modes along a branch with imaginary values of the frequency bounded below by $-\delta$ and above by $-\delta/2$, and again there are several prominent modes that are less dissipative (the noise in the upper left region is due to a convergence problem, discussed in [section 6](#)). As before, the gravest mode frequency is similar to that obtained with a long-wave solution.

The long-wave solution follows from integrating along the (zonal) characteristics from the eastern boundary (which is of course curved):

$$\psi_l = \Gamma \exp\{-i\omega F[x - (1 - y^2)^{1/2}]\},$$

$$(x^2 + y^2) \leq 1. \quad (29)$$

With weak damping, the mass integral is once again dominated by the interior contribution. The integral over the circle can be evaluated using a generating function and is

With the n^{-2} factor, the sum converges rapidly. The first three long-wave modes are indicated by the crosses in the upper panel of Fig. 7. As before, the frequencies of the gravest modes from the long-wave and the full solutions are nearly the same, though again the mismatch increases for successively higher modes.

To compare the structure of the gravest modes, we append the boundary layer correction:

$$\Psi = \psi_l + (\Gamma - \psi_l) \exp\{-d[x + (1 - y^2)^{1/2}]\}, \quad (31)$$

where

$$d \equiv \frac{\delta + \omega_i + i\omega_r}{(\delta + \omega_i)^2 + \omega_r^2}.$$

As with the long-wave solution in the tilted square, $\omega_i > -\delta$ is required to have a boundary layer on the western wall.

The gravest modes from the full and long-wave solution are contoured in the lower panels of Fig. 7, and we see they are very similar. This supports the contention that the weakly damped mode in the circular basin is of the long-wave type, as was the case in the tilted rectangular basin.

The long-wave modes thus occur in both tilted rectangular and circular basins. They occur when F is large, evidently so long as there is sufficient dissipation to damp small scales. The modes occur regardless of whether the basins is symmetric or asymmetric in y .

4. Forced response

The unforced evolution of a given flow is characterized by the spin down of modes onto which the initial streamfunction projects. The free modes though do not necessarily dominate the forced response, and it is the forced response that is more directly relevant to the ocean. We return to the tilted basin, but with forcing.

The method of solution of (9) with harmonic forcing follows closely that without forcing because the boundary oscillation there acted much like a forcing. With $\mathcal{T} = \exp\{ik[x \cos(\alpha) - y \sin(\alpha)] - i\omega t\}$, the solution is

$$\begin{aligned} \psi = \Gamma + \sum_{n=1}^{\infty} \left\langle \left\{ -[\gamma_1 e^{ikl \cos(\alpha)} + \gamma_2 e^{i(\kappa+k)l \cos(\alpha)}] \frac{\sin(a_n x)}{\sin(a_n l)} + (\gamma_1 + \gamma_2) \frac{\sin[a_n(x - l)]}{\sin(a_n l)} \right\} e^{-i\kappa[x \cos(\alpha) - y \sin(\alpha)]} \right. \\ \left. + \gamma_1 e^{iky \sin(\alpha)} + \gamma_2 e^{i[kx \cos(\alpha) + ky \sin(\alpha)]} \right\rangle \sin(n\pi y) \end{aligned} \quad (32)$$

with

$$\gamma_1 \equiv \frac{2\tilde{F}\Gamma n\pi[1 - (-1)^n e^{-i\kappa \sin(\alpha)}]}{[\kappa^2 \sin^2(\alpha) - n^2\pi^2 - \tilde{F}][n^2\pi^2 - \kappa^2 \sin^2(\alpha)]}$$

and

$$\gamma_2 \equiv \frac{4i\kappa n\pi[1 - (-1)^n e^{-i(\kappa+k) \sin(\alpha)}]}{[\kappa^2 - (\kappa + k)^2 \cos^2(\alpha) - n^2\pi^2 - \tilde{F}][n^2\pi^2 - (\kappa + k)^2 \sin^2(\alpha)]}.$$

(Click the equation graphic to enlarge/reduce size)

Again we obtain Γ by integrating over the basin. This (eventually) yields

$$\Gamma = \sum_{n=1}^{\infty} N_n / \left(l + \sum_{n=1}^{\infty} D_n \right), \quad (33)$$

where

$$\begin{aligned} N_n \equiv \gamma_2 g'_n \left\{ (ik \cos(\alpha) \sin(a_n l) [e^{ikl \cos(\alpha)} - 1] + a_n \cos(a_n l) [e^{ikl \cos(\alpha)} + 1] - a_n [e^{i(\kappa+k)l \cos(\alpha)} + e^{-ikl \cos(\alpha)}]) \right. \\ \left. + \frac{1}{ik \cos(\alpha)} [e^{ikl \cos(\alpha)} - 1] \right\} \end{aligned} \quad (34)$$

and where the denominator of (33), $l + \sum_n D_n$, is the dispersion relation (17).

Now the forcing determines the frequency ω , which is real. One indication of the strength of the response is the size of Γ , that is, the response at the “coast”; this is plotted versus forcing frequency for two values of tilt in Fig. 8. The left panels represent solutions with less dissipation ($\delta = 10^{-5}$) and the right with more dissipation ($\delta = 10^{-4}$). For simplicity, we consider forcing with the gravest zonal mode, that is, $k = 0$ (akin conceptually to seasonal forcing).⁵

Recall that without forcing, the gravest “long-wave” resonances for the case with $\alpha = \pi/12$ lie close to the axis with $\omega_i = 0$ (Fig. 4); one might therefore expect to see evidence of them with forcing and a purely real ω . This is the case (upper panels of Fig. 8). With both values of δ there are clearly defined peaks at frequencies near those for the free modes (Fig. 4). With less dissipation, the “lower branch” modes are also seen, but with more dissipation these are filtered out and the long-wave resonances dominate.

With $\alpha = \pi/5$, the lower-branch resonances are again evident with $\delta = 10^{-5}$, and even persist with $\delta = 10^{-4}$, but the long-wave resonances are greatly diminished. This too might have been anticipated from the unforced results; the long-wave modes with $\alpha = \pi/5$ are farther from the $\omega_i = 0$ axis (Fig. 4) and so, evidently, have a weaker projection there. We see two maxima near the expected gravest long-wave resonant frequencies, but these are weaker than the general response between $\omega = 0.006$ and $\omega = 0.009$.

So it seems fruitful to use the free modes to interpret the forced response. But the reader may have already noticed that the values of δ used for Fig. 8 are 10 and 100 times less than that used for Fig. 4! In fact, the level of dissipation is closer to that used for the upper panel of Fig. 6, where the long-wave resonances were not apparent at all. How can this be?

As suggested, the key issue is the extent to which the modes “project” onto the $\omega_i = 0$ axis. By comparing Figs. 8 and 4 it becomes clear that the long-wave modes *must exist even with weaker dissipation*. From Fig. 6 one is tempted to conclude they do not exist with $\delta < 5 \times 10^{-4}$, but from Fig. 8 the resonances are evident with δ as low as 10^{-5} (and possibly even less). In hindsight, we recognize that there are contours in Fig. 6 that extend up from the long-wave modes to the $\omega_i = 0$ axis, even when the modes are embedded in the lower branch. It seems that with forcing the question is to what extent the other lower-branch modes also project onto the real frequency axis, obscuring the long-wave modes.

The structural character of the forced waves is seen in Fig. 9. With $\omega = 0.0029$ (left panels), the wave closely resembles the gravest unforced mode, supporting our identification of the lowest peak in Fig. 8 with a long-wave mode (though the short-wave response is enhanced). But with $\omega = 0.0075$, the response is dominated by small scales and bears little resemblance to the third unforced long-wave mode (which has a mode-3 appearance in x). We expect that there is a connection, given that the resonant frequency matches that of the third long-wave mode, but in the very least the structure has been significantly altered. Recall that ω_i for mode 3 is more negative than for mode 1, suggesting a weaker projection onto the $\omega_i = 0$ axis.

Given that the long-wave resonances are less important for the more tilted square, we might infer a diminished role in more irregular basins. What then of the circular basin? That solution, with forcing $\exp(ikx - i\omega t)$, is

$$\psi = \sum_{n=0}^{\infty} B_n \cos(n\theta) J_n(\lambda r) e^{-i\alpha x} + C e^{ikx}, \quad (35)$$

where

$$B_n \equiv \frac{2i^n [\Gamma J_n(\alpha) - C J_n(k + \alpha)]}{(1 + \delta_{n0}) J_n(\lambda)},$$

$$C \equiv \frac{2i\alpha}{\lambda^2 - (k + \alpha)^2}, \quad \lambda^2 \equiv \alpha^2 - \bar{F},$$

and where $\alpha \equiv [2(\bar{\omega})]^{-1}$, as before.⁶ Invoking the mass integral constraint yields an expression for Γ . In the simpler case with $k = 0$, this is

$$\Gamma = C + \frac{i\alpha}{2D\lambda}, \quad (36)$$

where D is the sum given in (28).

Two solutions for Γ are shown in Fig. 10 for two values of δ . The response is very much like that in the tilted square in that both the long-wave resonances and “lower branch modes” (Fig. 7) are evident with weak dissipation. In fact, with $\delta = 10^{-3}$ the resonances (not shown) have amplitudes only slightly smaller than with $\delta = 10^{-4}$; the primary difference is that the gravest resonance is not resolved by the computation (sec. 6). Interestingly, this response resembles that in the untilted and less tilted ($\alpha = \pi/12$) square more than that in the more tilted ($\alpha = \pi/5$) square (Fig. 8) because the resonant peaks are more robust to dissipation. Since the zonal transit times differ greatly in the circle, it is therefore not true that a highly irregular basin implies weaker long-wave resonances.

One possible explanation of this is as follows. The forced, long-wave solution with $k = 0$ for a basin of arbitrary shape yields for Γ ,

$$\Gamma = \frac{1}{i\omega F} + \frac{A}{\left[L_y - \int_0^{L_y} e^{i\omega F L_x(y)} dy \right]}, \quad (37)$$

where A is the total area of the basin, $L_x(y)$ is the longitudinal width of the basin at latitude y and L_y is the total north–south extent of the basin. The square bracket in the denominator of (37) is the dispersion relation. For the long-wave modes, we expect $\omega F L_M \approx 2n\pi$, if $L_M = \max\{L_x(y)\}$; see, for example, (27). So the argument of the exponential in (37) is greater than or equal to 2π and the ability of the integral to balance the first term in the bracket is thus diminished.

However, if the basin possesses a point, or points in y where $L_x(y)$ is stationary as a function of y , the integral will be dominated by the contributions from those points in the standard fashion. Restricting the integral’s evaluation to a small neighborhood around such points reestablishes a one dimensional problem where the travel time that is important is the travel time at the stationary latitude. The circle has a single such point where the east–west extent is exactly the diameter of the circle. It is plausible that this is why the forced response of the circle so much resembles the untilted square. If correct, the response in realistic ocean basins might be dominated by a suite of modes generated at those latitudes where the basin width has a local stationary point.

To return to an earlier point, the forced response is greatly affected by the choice of boundary conditions. This is seen clearly in Fig. 10 of LaCasce (2000) for the untilted square with PV damping. In Fig. 11 we show similarly two forced solutions for the circular basin with RV damping with the two boundary conditions. The frequency, $\omega = 0.0035$, corresponds to the gravest maxima in Fig. 10. The response in the interior is similar in structure, but the amplitude of the $\Psi = \Gamma$ wave is more than an order of magnitude greater.

So the long-wave modes also influence the forced response, albeit with some variation with basin geometry. Even in cases where the free modes are less evident (as in the strongly tilted basin), the forced response is profoundly affected by the change in boundary conditions.

An important point was that the forced response showed evidence of long-wave resonances even when the dissipation was weak. From figures like Fig. 6, we concluded that the long-wave modes are thus not necessarily distinguished by a slow decay rate under scale-selective damping (but will be, of course, if the dissipation is strong).

5. PV damping

Now we consider what happens when the dissipation is not scale selective. Potential vorticity damping acts equally at all scales, so all modes decay at the imposed rate, $\omega_i = -\delta$. In fact, dissipation will also occur in the long-wave equation (19), so those solutions too must decay at the imposed rate.

Nevertheless, the long-wave modes (which do not exist when $\Psi = 0$ is imposed at the boundary) are important with PV damping, particularly with forcing. The 2D solution with PV damping is obtained as described above and modes for an untilted basin with $F = 2000$ are shown in the upper panel of Fig. 12. As expected, all frequencies have an imaginary part equal to $-\delta$; there are no “slowly decaying modes.”

However, there are modes whose real frequencies are very near the weakly damped modes found with RV damping. The gravest mode in the latter case had $\omega_r = 0.0029$, and the mode in Fig. 12 with the lowest frequency also has $\omega_r = 0.0029$ (similar counterparts are found for the higher weakly RV damped modes).

We tentatively identify this latter mode as the gravest long-wave mode for the PV-damped solution. Its streamfunction is shown in the lower panel. As with the gravest mode with RV damping (lower panel of Fig. 3), there is evidence of a large-scale feature, but there is also abundant small-scale variability. The latter presumably reflects that the damping has left the small scales intact.

It seems that with their faster decay rates, the long-wave modes with PV damping would be less important with forcing than with RV damping. This is true, to a degree. Shown in Fig. 13 is the boundary value of ψ versus forcing frequency in the weakly tilted square basin for the two types of damping, with two different damping coefficients. With $\delta = 10^{-4}$, the response is nearly the same; though the peak amplitudes are somewhat smaller with PV damping, resonances are clear in both cases. With $\delta = 10^{-3}$ however, resonances are clearly seen only with RV damping.

As before, the key issue is the extent to which the modes extend in frequency space to the $\omega_i = 0$ axis. Though the long-wave modes decay more rapidly under PV damping, the projection onto the $\omega_i = 0$ axis is nearly as great with $\delta = 10^{-4}$ as with RV damping. With $\delta = 10^{-3}$ though, the modes with PV damping have a much weaker projection.

A second point relates to the structure of the forced response. With PV damping, small-scale variability is retained in (what we identified as) the gravest mode. However, the structure of the forced response is largely the same with both types of dissipation. The streamfunction with PV damping at $\omega = 0.0029$ for the weakly tilted square (shown in Fig. 14) closely resembles that with RV damping (the upper left panel of Fig. 9). This somewhat surprising result suggests the small-scale structure does not “project” onto the $\omega_i = 0$ axis. From the forced perspective, the response is not greatly changed with PV damping, so long as the dissipation is not too large. This explains then why LaCasce (2000) found such profound changes in the forced response with the boundary condition, despite having used PV damping (see his Fig. 10). Note too that such a result might not have been anticipated by examining only the free modes.

6. Convergence

The full solutions converge slowly at low frequencies. This is why the gravest mode in Fig. 7 is evidently only half resolved, and also why there are discontinuities at low frequencies in Fig. 10 and in the lower-right panel of Fig. 8. Another example, for the circular basin with $F = 1000$ and $\delta = 10^{-3}$, is shown in the upper panel of Fig. 15. Here too the gravest long-wave mode has not been fully resolved, despite our having used 300 terms to evaluate (28). With $F = 2000$, the gravest mode is not resolved at all. What is the reason for this poor convergence?

The problem apparently stems from the boundary layer(s). As seen for example in Fig. 5, there are rapid oscillations in the western (and northern) boundary layers. The wavelength of these boundary wiggles, moreover, decreases with decreasing frequency (this is a common aspect, even with steady forcing; Pedlosky 1987). The rapid variations produce similar variations in the mass integral, and require a large number of Fourier modes to resolve.

To illustrate this, we took the circular basin long-wave solution with the boundary correction (31) and integrated it over the basin. The integral in the boundary layer was calculated directly; that is, we did not use asymptotic values from the interior solution, ψ_I . The result is, again, poor convergence at low frequencies (middle panel of Fig. 15). In fact, the convergence appears to be even worse than in the full solution (upper panel). Integrating only the interior solution yields the dispersion relation (30), which converges very rapidly; so the difficulty must lie with the boundary layer.

The greater the area occupied by the boundary layer, the greater its contribution to the mass integral, and the worse the convergence. A calculation like that for the middle panel but with $\delta = 0.002$ yields even worse results, whereas one with $\delta = 5 \times 10^{-4}$ is somewhat better.

With the long-wave solution, there are of course ways to get around the boundary layer difficulty. One can evaluate the mass integral using the method of stationary phase, which is ideally suited for such cases. Doing so, we obtain the bottom panel of Fig. 15. The modal frequencies are only slightly different than those obtained by evaluating (30), that is, by ignoring the boundary layer contribution altogether. (Recall that the solution with $\omega = 0$ corresponds to a solution which is trivially zero.) Unfortunately we have not found an analogous way of improving the convergence for the full solutions.

Thus, interestingly, there is a range of dissipation below which the free modes are not seen and above which they are difficult to resolve numerically. This gives the long-wave modes an elusive quality (making it less surprising that they were not observed earlier). The convergence problem worsens with larger F because there are then more long-wave modes at low frequencies.


7. Summary and discussion

We have reexamined free and forced baroclinic quasigeostrophic waves in basins. The weakly damped, large-scale basin modes found by Cessi and Primeau (2001) and LaCasce (2000) in a square basin were shown to exist as well in irregularly shaped basins. These modes owe their existence to oscillations in the boundary value of ψ ; that is, they do not occur when $\psi = 0$ is imposed at the boundary. They also require that the deformation radius be significantly smaller than the basin. Under these conditions, the full solution is well approximated by one with long Rossby waves in the interior and boundary layers on the incident walls. The forced response is also strongly affected by the choice of boundary conditions; imposing $\psi = 0$ there can reduce the wave amplitude by an order of magnitude.

The long-wave modes persist in irregular basins and so do not require a basin that has equal zonal transit times (like the

square basin). Primeau (2002) has likewise observed the modes in a trapezoidal basin. Nor do the modes require meridional symmetry: they exist in the untilted square and circular basins, which are symmetric, but also in the tilted rectangular basin, which is not. It seems, therefore, that these modes are a robust feature of the response, so long as F is large.

With RV damping, the decay rate of the long-wave modes does not depend to first order on the damping coefficient but depends instead on the geometry of the basin. With stronger dissipation, the modes decay more slowly than all other modes; with weaker dissipation, they evidently decay at a comparable rate. The extent to which the geometry influences the decay is not easy to predict a priori. The decay rate in the square basin increases with tilt; it also increases in a trapezoidal basin as the bottom is lengthened relative to the top (Primeau 2002). But fairly weak decay rates are found in the circular basin.

The existence of the long-wave free modes requires $\delta > O(F^{-1})$, as demonstrated by our numerical solutions (section 2c). As stated in sections 2a and 3, the necessary condition for the existence of the western (and northern, where applicable) boundary layers required to close the long-wave modal solutions is $\delta > -\omega_i$. Since $-\omega_i$ is $O(F^{-1})$ and independent of δ in the long-wave limit, this establishes $\delta > O(F^{-1})$ as the criterion. At first this seems counterintuitive (having enough friction for the existence of a free mode), but we recall that this is a criterion for the existence of the free mode of a special type. If the criterion is not satisfied, the short-wave energy generated by reflection at the western (and northern) boundaries is not trapped but penetrates the basin interior, as demonstrated by our free solutions for small δ . On the other hand, the forced solutions always have strictly real ω so that no such criterion is required for solutions which resemble the long-wave modes as we have seen (e.g., Fig. 9 )

The decay rates also influence the extent to which the free modes affect the forced response; the faster the decay, the less important they are. In a strongly tilted basin, the long-wave modes are evident but weak, and higher frequency modes (which do not differ much from those with zero boundary displacement) appear. But in the circular basin, the long-wave modes are again the dominant feature. This follows, we suggest, from the existence of an extremum in basin width (i.e., long-wave travel time) as a function of latitude.

We observed that PV damping, which acts equally at all scales, alters the free and forced response quantitatively, but not qualitatively. This is an important point because we do not know how PV is dissipated in the upper ocean. It is, however, certainly plausible that PV is removed at small scales, as it would be for example under a direct cascade of potential enstrophy. Then the long-wave resonances would also be weakly damped ones.

Of course, our “irregular” basins are still not nearly as complex as typical oceanic basins. But as long as F is large, we expect nothing fundamentally different with a more irregular geometry. Similarly it should not matter if the long-wave phase speed varies with latitude or if the Kelvin wave speed is finite. Primeau (2002) finds long-wave-type modes under the planetary geostrophic equations in a basin shaped like the Pacific.

In the real ocean, Kelvin waves have finite speeds and thus are susceptible to damping, which could in turn greatly weaken or defeat the weakly damped modes. Milliff and McWilliams (1994) found very similar adjustments to localized forcing with a primitive equation numerical model and one based on QG. Nevertheless, their domain was idealized, which perhaps lessened Kelvin wave damping. Certainly further work is required to know whether the weakly damped modes exist in realistic ocean models.

One concern though is whether such models can at present resolve these resonances. Our two-dimensional solutions demand a large number of Fourier modes, due to the boundary layers that are rich in small-scale structure when F is large and ω small. It is possible that oceanic GCMs must resolve small scales to a comparable degree in order to capture these large-scale features.

Acknowledgments

We thank F. Primeau, P. Cessi, and M. Spydell for graciously sharing their preliminary results with us. Karl Helfrich and two anonymous reviewers made helpful comments on the manuscript. LaCasce was supported in part by an ONR SECNAV Scholarship. Pedlosky was supported in part under NSF OCE9901654.

REFERENCES

Cessi P., and F. Primeau, 2001: Dissipative selection of low-frequency modes in a reduced-gravity basin. *J. Phys. Oceanogr.*, **31**, 127–137. [Find this article online](#)

Flierl G. R., 1977: Simple applications of McWilliams' “A note on a consistent quasigeostrophic model in a multiply connected domain.”. *Dyn. Atmos. Oceans*, **1**, 443–453. [Find this article online](#)

LaCasce J. H., 2000: Baroclinic Rossby waves in a square basin. *J. Phys. Oceanogr.*, **30**, 3161–3178. [Find this article online](#)

Longuet-Higgins M. S., 1964: Planetary waves on a rotating sphere. *Proc. Roy. Soc. London*, **279A**, 446–473. [Find this article online](#)

McWilliams J. C., 1977: A note on a consistent quasigeostrophic model in a multiply connected domain. *Dyn. Atmos. Oceans*, **1**, 427–441.

[Find this article online](#)

Milliff R. F., and J. C. McWilliams, 1994: The evolution of boundary pressure in ocean basins. *J. Phys. Oceanogr.*, **24**, 1317–1338. [Find this article online](#)

Pedlosky J., 1965: A study of the time dependent ocean circulation. *J. Atmos. Sci.*, **22**, 267–272. [Find this article online](#)

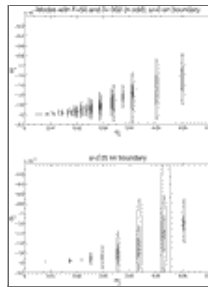
Pedlosky J., 1987: *Geophysical Fluid Dynamics*. Springer-Verlag, 710 pp.

Phillips N., 1966: Large-scale eddy motion in the western Atlantic. *J. Geophys. Res.*, **71**, 3883–3891. [Find this article online](#)

Primeau F., 2002: Long Rossby wave basin-crossing time and the resonance of low-frequency basin modes. *J. Phys. Oceanogr.*, **32**, 2652–2665. [Find this article online](#)

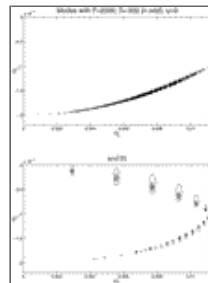
Stommel H., and G. Veronis, 1956: The action of variable wind stresses on a stratified ocean. *J. Mar. Res.*, **15**, 43–75. [Find this article online](#)

Figures



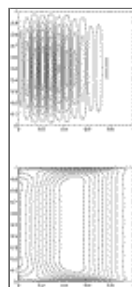
[Click on thumbnail for full-sized image.](#)

FIG. 1. Solutions to the dispersion relation (17) for an untilted square basin with $F = 50$ and $\delta = 0.002$: (upper panel) $\psi = 0$ was imposed on the boundary and (lower panel) $\psi = \Gamma(t)$. The contours are for the modulus of the sum, with the bull's-eyes indicating the minima. Only modes corresponding to odd-numbered sine terms in y are shown in the upper panel, as described in the text



[Click on thumbnail for full-sized image.](#)

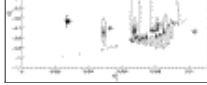
FIG. 2. As in [Fig. 1](#) but with $F = 2000$. Note the maximum free wave frequency, $(2(F)^{1/2})^{-1}$, is 1.1×10^{-2}



[Click on thumbnail for full-sized image.](#)

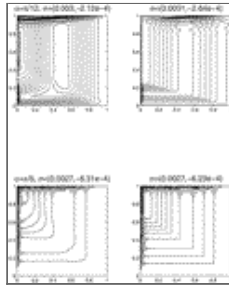
FIG. 3. Streamfunction contours for the gravest modes in [Fig. 2](#). The contour values are $\pm[-2, -1.5, -1, \dots, 1.5, 2]$





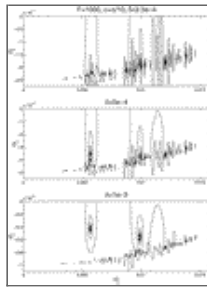
Click on thumbnail for full-sized image.

FIG. 4. Solutions to the dispersion relation (17) for the tilted square with two tilt angles: (top) $\alpha = \pi/12$ and (bottom) $\alpha = \pi/5$. The crosses in both panels are solutions obtained from the long-wave solution discussed in section 2a



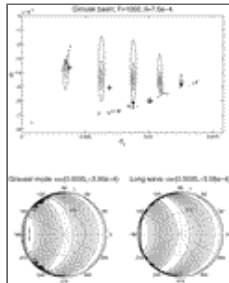
Click on thumbnail for full-sized image.

FIG. 5. (left) Streamfunction contours for the gravest modes in Fig. 4 with those obtained from (right) the long-wave solution. The contour values are as in Fig. 3.



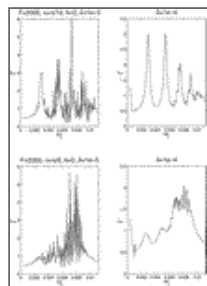
Click on thumbnail for full-sized image.

FIG. 6. Solutions to the dispersion relation (17) for the tilted square with $\alpha = \pi/10$, $F = 1000$, and three values of δ



Click on thumbnail for full-sized image.

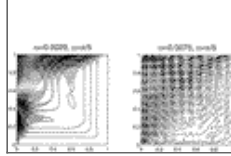
FIG. 7. (top) Solutions to the dispersion relation (28) for a circular basin. The crosses again indicate solutions from the long-wave solution. Note the region of poor convergence at low frequencies. (bottom) The gravest mode streamfunctions from (left) the full calculation and (right) the long-wave solution.



Click on thumbnail for full-sized image.

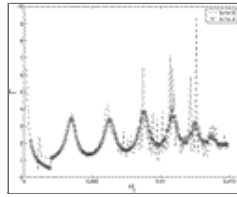
FIG. 8. The value of Γ vs forcing frequency for the tilted square basin with zonally nonvarying forcing ($k = 0$) and $F = 2000$. Two values of tilt and of δ are shown





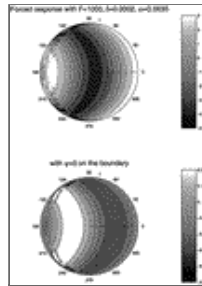
Click on thumbnail for full-sized image.

FIG. 9. The streamfunctions for two forcing frequencies with the parameters as in Fig. 8 and $\delta = 10^{-4}$



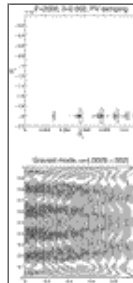
Click on thumbnail for full-sized image.

FIG. 10. Response Γ vs forcing frequency for the circular basin with $\delta = 10^{-5}$ and $\delta = 10^{-4}$. Again $F = 1000$ and $k = 0$ (the forcing is zonally nonvariant)



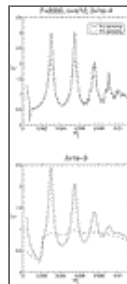
Click on thumbnail for full-sized image.

FIG. 11. Streamfunctions from the forced circular basin with (top) $\psi = \Gamma$ and (bottom) $\psi = 0$ imposed on the boundary. The parameters were as shown



Click on thumbnail for full-sized image.

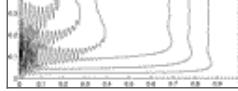
FIG. 12. The solutions to the dispersion relation (17) for the untitled square under PV damping. (upper panel) The free modes and (lower panel) the streamfunction of the mode with $\omega_p = 0.0029$



Click on thumbnail for full-sized image.

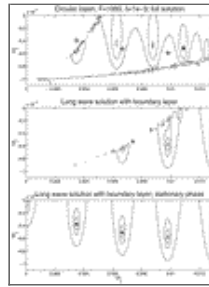
FIG. 13. Plot of Γ vs forcing frequency for the tilted square with $\alpha = \pi/12$, $F = 2000$, and two values of dissipation. The solid lines indicate RV damping and the dashed PV damping





Click on thumbnail for full-sized image.

FIG. 14. Streamfunction contours for the gravest mode in Fig. 13 for forced response; $\delta = 1 \times 10^{-4}$, PV damping. Compare the structure with that in the upper-left panel of Fig. 9; the contour values are the same as in Fig. 3



Click on thumbnail for full-sized image.

FIG. 15. The solutions to the dispersion relation in the circular basin with $F = 1000$ and $\delta = 10^{-3}$: (upper panel) the full solution, (middle panel) the modes found by integrating the long-wave solution plus the boundary layer contribution, and (lower panel) the modes obtained by integrating the boundary layer term by stationary phase. Note the convergence problem, which affects the full solution, also occurs with the long-wave solution, indicating it is due to the boundary layer.

* Woods Hole Oceanographic Institution Contribution Number 10568

Corresponding author address: Joe LaCasce, Norwegian Meteorological Institute, P.O. Box 43, Blindern, 0313 Oslo, Norway. E-mail: jlacase@met.no

¹ We learned that P. Cessi and M. Spydell were also working on baroclinic waves in a tilted square basin: they graciously showed us some of their results.

² Observe that, if $\Gamma = 0$, the modes do not depend on the tilt angle, α .

³ It is straightforward to prove that the imaginary part of the frequency is bounded below by $-\delta$ in all cases.

⁴ Primeau (2002) similarly uses the long-wave solution to calculate the resonant frequencies in the trapezoidal basin.

⁵ We will not examine the dependence on k , which is much like that in the untilted basin, discussed by LaCasce (2000). It is, however, the forcing frequency that is more important with regard to resonant excitation.

⁶ The solution was obtained without separating out the boundary contribution, as in (12), so that Γ does not appear in (35) as an additive correction. Nevertheless $\Psi = \Gamma$ at $r = 1$, as is easily confirmed.

top ▲



© 2008 American Meteorological Society [Privacy Policy and Disclaimer](#)
 Headquarters: 45 Beacon Street Boston, MA 02108-3693
 DC Office: 1120 G Street, NW, Suite 800 Washington DC, 20005-3826
amsinfo@ametsoc.org Phone: 617-227-2425 Fax: 617-742-8718
[Allen Press, Inc.](#) assists in the online publication of AMS journals.